Presented at the 38th European PV Solar Energy Conference and Exhibition, 6-10 September 2021

DESIGN AND DEVELOPMENT OF SOLAR CELL INTEGRATED MOISTURE AND TEMPERATURE SENSORS FOR PHOTOVOLTAIC MODULES

Jaimin Navin Bhai Patel[1], Esther Fokuhl[1], Karthika Sheeja Prakash[1], Andreas Beinert[1], Viktor Wesselak[2], Paul Gebhardt[1], Daniel Philipp[1]
[1] Fraunhofer Institute for Solar Energy Systems Heidenhofstr. 2, 79110 Freiburg, Germany
[2] Institute for Renewable Energy Technologies (in.RET), University of Applied Sciences Nordhausen, Weinberghof 4, D-99734 Nordhausen, Germany

ABSTRACT: We are presenting the design and development of a capacitive moisture sensor and a resistive temperature sensor integrated into solar cells. The sensors are produced by screen printing on solar cell wafers using a silver paste commonly used in solar cell production. The sensor cells are designed to be integrated into PV modules. For evaluation of the sensors, measurements of imprinted wafers laminated between two layers of encapsulant were performed. Impedance measurements on the moisture sensor indicate an exponential dependency of the capacitance on the moisture content in the encapsulant at constant temperatures. The temperature sensors show a high sensitivity and reproducibility.

Keywords: Capacitance, Impedance, Resistance, Moisture, Temperature, Screen Printing, Sensor

1 INTRODUCTION

Degradation of PV modules under long-term operational conditions can be attributed to different climatic conditions like humidity, high temperature, Ultraviolet (UV) irradiation, temperature changes, and mechanical stress. Out of these, moisture ingress and high temperature are important environmental factors that are influenced by the climatic conditions on-site and the PV module design. The moisture typically penetrates from the back sheet and from the module edges through the encapsulation polymers. It can lead to electrochemical corrosion of cells and metallization as well as yellowing of the encapsulant [1]. High and low temperature cycles can cause thermomechanical fatigue and cracks in the cell, and broken interconnectors [2]. High cell temperature reduces the efficiency of the module [3].

Huyberechts et al. enabled humidity monitoring inside of PV modules using alumina substrates containing screen-printed interdigitated electrodes [4]. The permittivity of the polymer was monitored by electrochemical impedance spectroscopy. Carlsson et al. monitored moisture ingress into a polymer by using a conductive coating and a fork-type geometry on a glass substrate acting as the moisture-sensitive component [5]. Jankovec et al. developed an in-situ measurement technique based on commercial digital humidity sensors laminated in PV-module-like structures and mini-modules [6]. For the latter approach, the module EVA thickness had to be adapted to the commercial humidity sensors, because of their size.

As an advantage over these sensor concepts, the solar cell integrated sensor presented in this work can be produced with standard screen-printing processes by using materials common in solar cell production and are an extension to the previously presented solar cell integrated stress sensors [7]. Therefore, the sensor cell can be easily integrated with other solar cells into the module. PV module integrated moisture and temperature sensors can help to understand the root causes of degradation in the field and indoor tests by monitoring stress due to moisture and temperature.

2 APPROACH

2.1 Humidity sensor design

An interdigitated capacitor with comb-shaped electrodes is used as moisture sensor. Ethylene-vinyl acetate (EVA), which is used as encapsulant in our experiments, functions as dielectric of the capacitor. A schematic diagram of the humidity sensor is presented in Figure 1. The design parameters were chosen based on requirements of the printing process and calculations on the expected capacitance values as listed in Table 1.

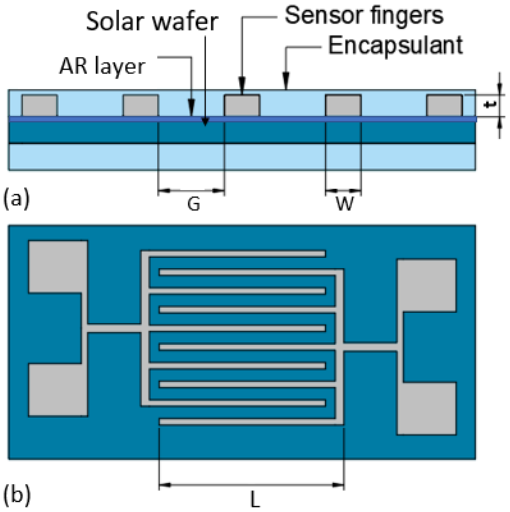

Figure 1: Schematic drawing of the moisture sensor (a) Cross-sectional view of sensor electrodes on a solar wafer laminated between two sheets of encapsulant (b) Top view of the sensor. L, W, and t are the length, width, and thickness/height, where G is the spacing between the fingers.

Table 1: Design parameters of the humidity sensor.

Parameters	
Number of fingers (N)	10
Length of electrode (L)	5 mm
Gap between fingers (G)	200 µm
Width of the finger (W)	60 µm
Thickness of the finger (t)	20 µm

2.2 Temperature sensor design

The design of the temperature sensor is based on the principle of resistance temperature sensors. A similar approach with a meander-shaped structure and a lower printing height, which led to PT-100-like characteristics, has been evaluated in previous work [7]. In this work, we are using the same paste and printing process as used for the humidity sensors and therefore chose a simplified design for the temperature sensor as shown in the schematic diagram in Figure 2.

The parametric equation for resistance depends on the length (L), cross-section (A), and resistivity (ρ) of the material:

$$R = \rho \frac{L}{A} \qquad (1)$$

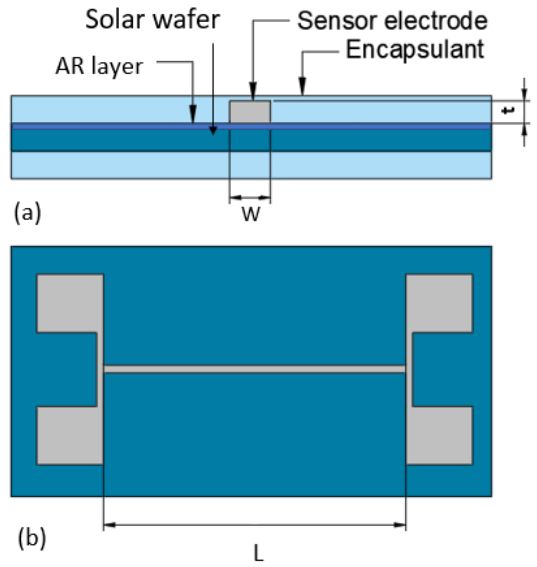

Figure 2: Schematic drawing of the temperature sensor (a) Cross-sectional view of the sensor on a solar wafer laminated between two sheets of encapsulant (b) Top view of the sensor. L, W, and t are the length, width, and thickness/height of the electrode.

The design dimensions for the temperature sensor are listed in table 2.

Table 2: Design parameters of temperature sensor

Parameters	
Width of the finger (W)	60 µm
Length of the electrode (L)	13.75 mm
Thickness of the electrode (t)	20 µm

Resistance values of the conductor at any temperature are determined by the below equation (2),

$$R = R_{ref}\left(1 + \alpha\left(T - T_{ref}\right)\right) \qquad (2)$$

Where R is the resistance at temperature T in Ω, R_{ref} is the resistance at reference temperature T_{ref} in Ω, T is the temperature in °C, T_{ref} is the reference temperature in °C (usually 20 °C), and α is the temperature coefficient of resistance for the material. For calibration purposes, a quadratic polynomial equation is used and it is defined for PT-100 temperature sensors in IEC 60751.

3 EXPERIMENT SETUP

3.1 Sample preparation

The sensors are printed on the front side of solar wafers by using a screen-printing process. In this experiment, low-temperature and high-temperature silver paste are used for the metallization of the sensor. After the screen printing of the sensors, the wafers are cut horizontally into 4 strips with a laser. The sensing part is connected by soldering high-temperature resistive wires to the contact pads.

To enable a fast moisture ingress and egress into the samples and therefore faster moisture content changes in the polymeric material at the sensor locations, the sensor stripes were laminated between two layers of EVA without front glass and polymeric back sheet. To monitor reference values for the moisture inside the laminates during the climate chamber investigations, a commercial humidity sensor (SHT31D) was also placed next to the wafer strips between the EVA sheets (see Figure 3 (c)). The lamination of the samples was carried out in a standard lamination process for PV modules with a lamination time of 25 minutes and a lamination temperature of 160 °C.

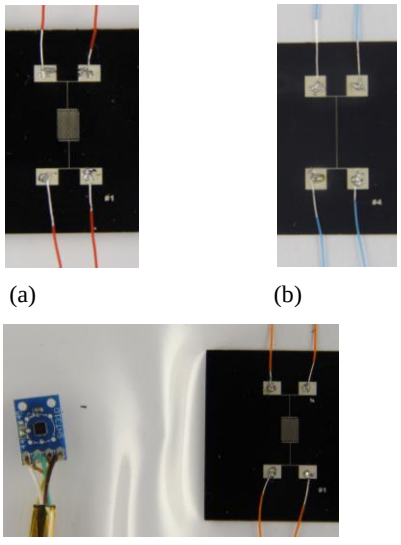

(a) (b)

(c)

Figure 3: (a) laminated screen-printed humidity sensor (b) laminated screen-printed temperature sensor (c) commercial humidity sensor laminated between the EVA sheets with a sensor strip.

3.2 Measurement setup

For the measurement of the capacitive values of the humidity sensor, an LCR meter was used, which measures the real and imaginary components of

impedance. The effective test voltage used for this experiment is 1 V. For the capacitance analysis, 100 Hz, 120 Hz, 1 kHz, 10 kHz, and 100 kHz frequencies were applied. An automated measurement setup [8] was used as shown in Figure 4. A data logger (Agilent 34970A) was connected to the LCR meter. The data logger had three measurement cards, which were used as switch units in this setup. This way, numerous test samples can be monitored simultaneously.

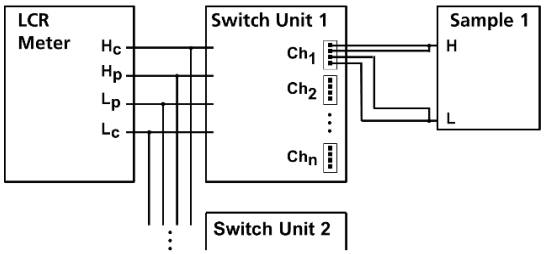

Figure 4: Schematic diagram of the LCR meter setup. Where Ch is demonstrated as Channels; Hc – High current; Hp – High potential; Lp – Low potential; Lc – Low current [8].

The resistance of the temperature sensors was measured by a multifunction device (Agilent 34980A), which contains a multimeter and a datalogger.

3.3 Test conditions

In order to evaluate the sensors, a range of environmental conditions were defined and controlled in a climate chamber.

The temperature range was set from -40 °C to 85 °C for the evaluation of the temperature sensor. The temperature inside the chamber was changed in steps of 20 °C for every step between -40 °C and 80 °C and a step of 5 °C between 80 °C and 85 °C. The holding time at constant temperature was approximately 2 h in this experiment. To verify the reproducibility of the sensor performance, the test between 20 °C to 85 °C was repeated once.

For the humidity sensors, the relative humidity was controlled in steps between 20 %RH and 85 %RH at constant temperatures of 85 °C and 60 °C. The humidity inside the chamber was changed in steps of 10% RH for every step between 20 %RH and 80 %RH and a step of 5 %RH between 80 %RH and 85 %RH. The holding time at constant relative humidity was approximately 1 h and 30 min at 85 °C and 2 h and 30 min at 60 °C. To investigate the reproducibility of the sensor response, the test at 85 °C was repeated 5 times ("five-cycle test").

4 TEST RESULTS

4.1 Setup capacitance

The sensors are not directly connected to the measurement device. The electrical properties of wires and datalogger cards (see Figure 4) contribute to the measured capacitance [8]. The measurement setup showed capacitive behaviour with a phase shift between voltage and current of $\varphi \approx 90°$ [8]. Thus, these parts of the measurement are considered as setup capacitance C_S, which is parallel to the sample. From this assumption, we can correct the capacitance of the sensor by subtracting C_S from the measured capacitance values C_{measured}. For a cable length of 2 m, C_S amounts approximately 355 pF ± 5 pF with neglectable humidity and temperature dependence.

4.2 Capacitance measurement of the humidity sensor

The test conditions used for analysing the humidity sensor are described in section 3.3. Only the sensors printed with low-temperature paste (LTP) are evaluated since the characterization of the high-temperature paste (HTP) sensors showed a low insulation resistance between the electrodes. This was most likely caused by the firing step, which was performed at a temperature between 800 °C and 850 °C. Therefore, the insulation effect of the AR layer is reduced because the AR layer deposition process (PECVD) was held at temperature between 165 °C to 400 °C [9].

Figure 5 shows the corrected capacitance values (after subtracting C_S) of a sensor printed with low-temperature paste. The measurements were taken with different frequencies at 85 °C and relative humidity setpoints between 20 % and 85 %RH. The humidity values on the x-axis correspond to the values measured by the commercial humidity sensor inside the sample after reaching a steady state.

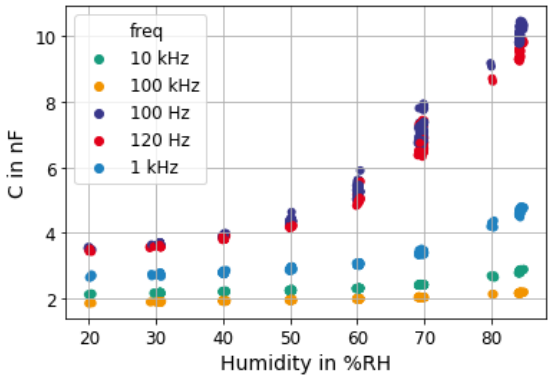

Figure 5: Sensor response at different frequency levels.

The capacitance values of a sensor was measured at different frequencies with increasing humidity. At 10 kHz and 100 kHz, the sensitivity is significantly lower than at lower frequency levels. At 100 Hz and 120 Hz, comparably high fluctuations of the measurement values were observed at humidity values above 50 %RH. The measurement values at 1 kHz represent a compromise with a moderate sensitivity and a comparably low fluctuation and were therefore used for further evaluation.

Figure 6 illustrates the capacitance values of a humidity sensor determined at 1 kHz and different humidity levels during the five-cycle test at 85 °C. The sensor response at constant temperature can be described by an exponential fit:

$$C = m + Ae^{B\%RH} \qquad (3)$$

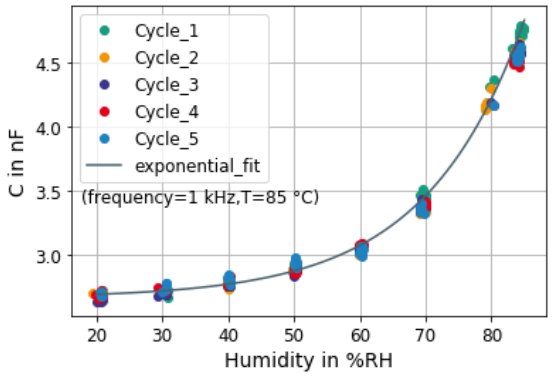

Figure 6: Measured capacitance of humidity sensor at 1 kHz frequency with exponential curve fit of the five-cycle test at 85 °C.

Additional measurements were performed at 60 °C and different steps of RH. Figure 7 shows the sensor measurements at 85 °C (first cycle measurement data from 5-cycle tests) and 60 °C. The sensor response shows similar behaviour at 60 °C as at 85 °C but with lower sensitivity to changes in relative humidity and with lower values at dry conditions. The lower sensitivity at 60 °C can be explained by the absolute moisture content, which is lower at the same RH values.

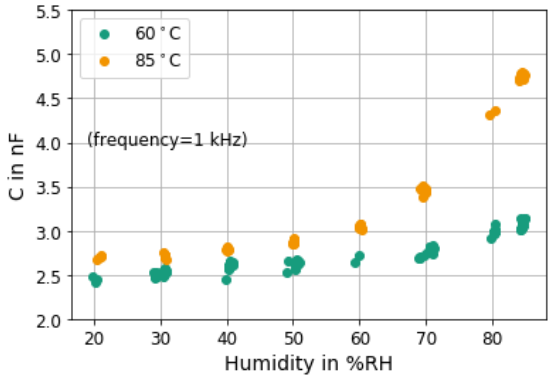

Figure 7: Capacitance measurement at different temperatures (e.g., 60 °C and 85 °C) at 1 kHz.

4.3 Resistance measurement of the temperature sensor

In order to characterize the temperature sensor, the resistance of the sensor was measured at different temperature ranges. Figure 8 and Figure 9 represent readings of the high-temperature paste and low-temperature paste printed sensors. In contrast to the humidity sensor, the firing step used for the high-temperature paste printed sensors had no negative effect because a high insulation resistance between paste material and wafer is not necessary for this measurement.

The sensor response of both pastes is different because of their different temperature coefficient of resistance α. The measured resistance changes within 20 °C steps are at least 4 % for the low-temperature paste and 5 % for the high-temperature paste printed sensor.

The sensors were calibrated using a method for PT-100 temperature sensors, according to IEC 60751. The resistance values at the temperature setpoints were fitted to the following polynomial equation:

$$R_{calculated} = R_0(1 + At + Bt^2) \qquad (4)$$

Where, R_0 is the reference resistance at 0 °C, A and B are polynomial constants. Table 3 shows the constant values of high- and low- temperature paste.

Table 3: Constant values of polynomial fitted curve

	LTP	HTP
R_0	0.926	0.489
A	3.23e-3	3.86e-3
B	3.82e-7	-3.58e-7

The resistance value at reference temperature R_0 varies because of different temperature co-efficient for both pastes (see equation (2)). The constants A and B show similarities in values but the polarity is different for constant B.

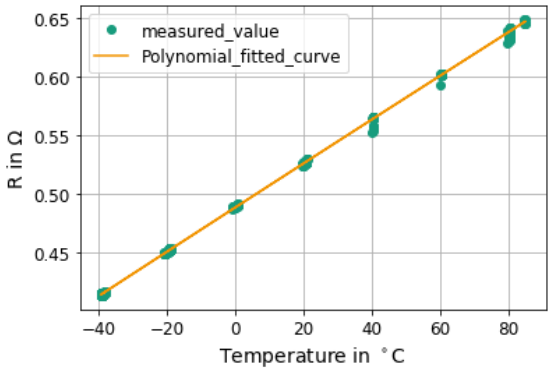

Figure 8: Temperature dependent resistance of a sensor, which was printed with high-temperature paste

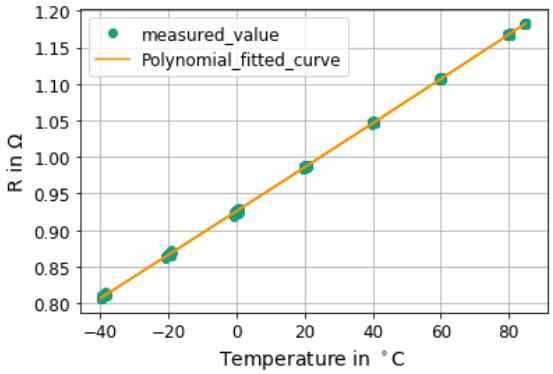

Figure 9: Temperature dependent resistance of a sensor, which was printed with low-temperature paste

The experiment with low-temperature paste was repeated to investigate the reproducibility of the temperature sensor (see Figure 10). The measured values are reproducible at the tested temperature range.

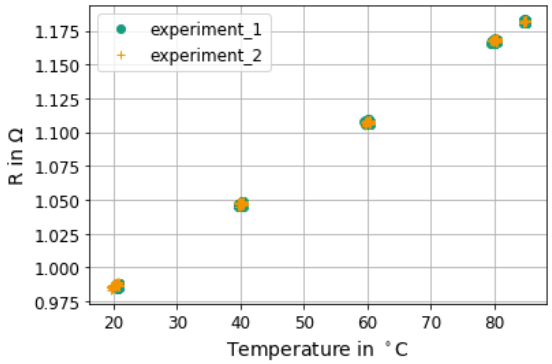

Figure 10: Temperature dependent resistance values from two experiments (low-temperature paste sensor); where experiment_1 is at temperatures between -40 °C and 85 °C test data points and experiment_2 is at temperatures between 20 °C to 85 °C test data points

5 SUMMARY AND OUTLOOK

We have presented the design and proof of concept of screen-printed, solar cell integrated humidity and optimized temperature sensors.

The humidity sensor was analysed under different relative humidity conditions between 20 %RH and 85 %RH at constant temperatures of 85 °C and 60 °C. The sensor gives an exponential response to increasing moisture in the EVA and shows high reproducibility. The temperature sensor was evaluated at temperatures between -40 °C and 85 °C. The sensor gave a polynomial response, following the calibration function according to IEC 60751, and showed high reproducibility.

As a further step, a full calibration of the humidity sensors is planned. Since the measurement values of the humidity sensor are not solely humidity dependent but also change with temperature, calibration steps at various temperature levels are required. In the future, both the temperature and the humidity sensor are planned to be integrated into PV modules for experimental purposes and on-field measurements. For the application on-field, a new measurement setup, ideally with wireless data transmission, will be needed.

6 ACKNOWLEDGEMENTS

The authors would like to thank Denis Erath, Michael Linse, Timo Wentzel, Diana Witt, Georg Mülhöfer, Heinrich Berg, Sandor Stecklum and Felix Basler for sample preparation, technical help and insightful discussions during experiment works.

7 REFERENCES

[1] Bouaichi A, Merrouni AA, El Hassani A, Naimi Z, Ikken B, Ghennioui A, Benazzouz A, El Amrani A, Messaoudi C. Experimental evaluation of the discoloration effect on PV-modules performance drop. *Energy Procedia* 2017;119:818–27, doi:10.1016/j.egypro.2017.07.107.

[2] Quansah DA, Adaramola MS, Takyi G. Degradation and longevity of solar photovoltaic modules—An analysis of recent field studies in Ghana. *Energy Sci Eng* 2020;8:2116–28, doi:10.1002/ese3.651.

[3] Razak A, Irwan Y, Leow WZ, Irwanto M, Safwati I, Zhafarina M. Investigation of the Effect Temperature on Photovoltaic (PV) Panel Output Performance. *International Journal on Advanced Science, Engineering and Information Technology* 2016;6:682, doi:10.18517/ijaseit.6.5.938.

[4] Guido Huyberechts LF. In situ formation of humidity-sensitive devices for the evaluation of solar panel encapsulations.

[5] Carlsson T, Halme J, Lund P, Konttinen P. Moisture sensor at glass/polymer interface for monitoring of photovoltaic module encapsulants. *Sensors and Actuators A: Physical* 2006;125:281–7, doi:10.1016/j.sna.2005.07.022.

[6] Marko Jankovec, Eleonora Annigono, Christophe Ballif, Marko Topič. In-situ Determination of Moisture Diffusion Properties of PV Module Encapsulants Using Digital Humidity Sensors. *IEEE J. Photovoltaics* 2018.

[7] Beinert AJ, Imm M, Benick J, Becker F, Seitz S, Heinrich M, Paul O, Glunz SW, Aktaa J, Eitner U, Neuhaus H. Silicon solar cell–integrated stress and temperature sensors for photovoltaic modules. *Prog Photovolt Res Appl* 2020;28:717–24, doi:10.1002/pip.3263.

[8] Esther Fokuhl, Heinrich Berg, Sandor Stecklum, Djamel Eddine Mansour, Daniel Philipp, Paul Gebhardt. MONITORING THE MOISTURE INGRESS INTO PV MODULES BY MEASURING CAPACITIVE CHARACTERISTICS. *European Photovoltaic Solar Energy Conference and Exhibition (EU PVSEC)* 2020.

[9] Yimao Wan, Keith R. McIntosh, and Andrew F. Thomson: Characterisation and optimisation of PECVD SiNx as an antireflection coating and passivation layer for silicon solar cells (*AIP Advances* 3, 032113 (2013)).